Probing Intermolecular Coupled Vibrations between Two Molecules

Zhumin Han (韩竹敏),[1] Gregory Czap,[1] Chen Xu (徐晨),[1] Chi-lun Chiang (蔣季倫),[1] Dingwang Yuan (袁定旺),[1,2] Ruqian Wu,[1] and W. Ho[1,3,*]

[1]Department of Physics and Astronomy, University of California, Irvine, California 92697-4575, USA
[2]Center for High Resolution Electron Microscopy, College of Materials Science and Engineering, Hunan University, Changsha 410082, China
[3]Department of Chemistry, University of California, Irvine, California 92697-2025, USA

(Received 16 November 2016; published 19 January 2017)

Intermolecular interactions can induce energy shifts and coupling of molecular vibrations. However, the detection of intermolecular coupled vibrations has not been reported at the single molecule level. Here we detected an intermolecular coupled vibration between two CO molecules, one on the surface and another on the tip within the gap of a subkelvin scanning tunneling microscope, and analyzed the results by density functional calculations. We attribute the evolution of the energy and intensity of this coupled vibration as a function of tip-sample distance to the tilting and orbital alignment of the two CO molecules.

DOI: 10.1103/PhysRevLett.118.036801

The study of the adsorption and reaction of carbon monoxide (CO) molecules has played an important role in the development of modern surface science [1]. Recently, the attachment of CO to the tip in noncontact atomic force microscopy (NC-AFM) [2–4] and the inelastic tunneling probe (itProbe) with the scanning tunneling microscope (STM) [5] have revealed submolecular structures of single adsorbed molecules. Functionalizing the scanning probe tip with a flexible molecule is the key to obtaining enhanced spatial resolution in these methods. Furthermore, the system consisting of a CO molecule on the surface and another on the tip has served as a model for probing intermolecular interactions by normal-force AFM [6,7] and lateral force microscopy (LFM) [8].

The vibrations of an adsorbed molecule are fingerprints for its chemical identification and reflect the nature of its interactions with the environment. Vibrational spectroscopy can be achieved at the single molecule level by inelastic electron tunneling spectroscopy (IETS) with the STM [9]. STM-IETS has been demonstrated to be a powerful tool not only for studying chemical bonds that molecules form with their environment, but also for studying intermolecular interactions by measuring the energy shift of molecular vibrations [5,10,11]. However, the emergence of intermolecular coupled vibrations, to our knowledge, has not been reported. The adsorbed CO molecule exhibits low energy hindered vibrations that are especially sensitive to interactions with its local environment. By monitoring the IETS intensity variations due to the energy shift of the CO-tip hindered translational mode, itProbe has been developed to image the chemical structure of planar molecules [5,12]. In addition, CO has served as the benchmark to understand STM-IETS, such as the propensity rules for mode intensity [13,14], spectral line shape [15,16], and spectroscopy with a functionalized tip [14,17]. Therefore, using a CO tip to probe another nonplanar CO on the surface presents an ideal system for vibrational spectroscopy with STM-IETS to gain new insights into intermolecular interactions.

Here we demonstrate the first detection of an intermolecular coupled vibrational mode with STM-IETS. This coupled mode was induced by short range intermolecular repulsion between an adsorbed CO on the Ag(110) surface and a CO attached to a Ag tip. Density functional calculations reveal that the new vibrational mode is an optical branch of the coupled translation mode of the CO dimer in junction. We tuned the CO-CO intermolecular interaction by adjusting the tip-sample distance and found that the vibrational energy and IETS intensity of this coupled mode do not change monotonically as the two CO molecules approach each other.

The experiment was performed with a home built, subkelvin STM in ultrahigh vacuum with base pressure of 5×10^{-11} Torr. The microscope scanner was adapted from the design of a variable temperature STM [18]. Both the Ag(110) surface and the electrochemically etched silver tip were prepared by repeated Ne^+ sputtering and annealing. The CO molecules were introduced to the surface at 25 K through a variable leak valve to obtain ~0.02 monolayer surface coverage. The sample was then cooled down to 600 mK for taking images and spectra.

Dark depressions were imaged for CO molecules on Ag(110) with a metal tip as shown in Fig. 1(a). With a CO-terminated tip, another CO on surface was imaged as a protrusion at the center surrounded by dark lobes and a bright circular border as shown in Fig. 1(b) [17,19]. In another topography obtained at smaller tunneling gap displayed in Fig. 1(c), the adsorbed CO molecule is imaged as four bright lobes at the center and surrounded by a circular border. Additionally, individual surface silver atoms were resolved, revealing the adsorption of CO on top of a Ag atom (the atop site) on the Ag(110) surface.

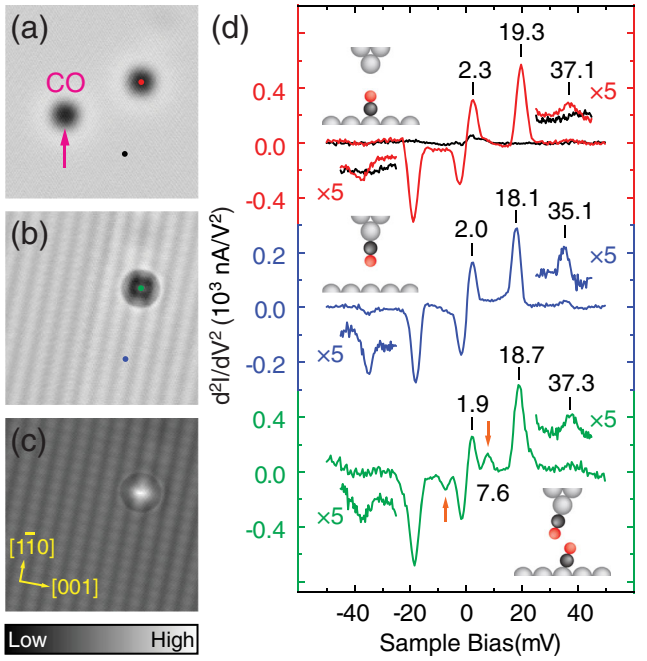

FIG. 1. STM topographies and vibrational IETS of CO on Ag(110). (a) STM constant current topography (45 Å × 45 Å) of CO molecules adsorbed on Ag(110) surface scanned with a bare Ag tip, the tunneling set point is 0.1 nA and 10 mV. (b) and (c) Constant current topographies of the same area with a CO-terminated tip at 0.1 and 0.5 nA/10 mV. The CO molecule transferred to the tip is indicated with the magenta arrow in (a). (d) d^2I/dV^2 STM-IETS for a bare Ag tip over Ag(110) as background (upper curves in black), Ag tip over CO/Ag(110) (upper curves in red), CO tip over Ag(110) (middle curves in blue) and CO tip over CO/Ag(110) (bottom curves in green). The schematic diagrams of the three tunneling junctions are displayed in the insets. The magnified (×5) IETS feature near 35 meV is obtained with finer bias step size and more averaging passes. For all spectra: sample bias modulation is 2 mV_{rms} at 311.11 Hz, tunneling gap set with 0.17 nA/10 mV for the Ag tip and 0.1 nA/10 mV for the CO tip.

The presence of CO on the surface or the tip apex can be verified by detecting its characteristic low energy vibrations with STM-IETS as shown in Fig. 1(d). The d^2I/dV^2 IETS taken with a bare Ag tip over a CO molecule and a CO tip over the clean Ag(110) surface show three vibrational modes. In addition to the hindered translation (HT, ~2 meV) and hindered rotation (HR, ~20 meV) as reported before [5,12,15,17], another mode at 37.1 meV for the surface CO and 35.1 meV for the tip CO was resolved. This energy is ~5 meV higher than that previously reported for the center of mass (c.m.) bouncing mode (Ag-CO stretch) [20,21] and our DFT calculations in Fig. S1. However, it is very close to twice the HR energy. Furthermore, the IETS cross section of the c.m. mode is expected to be very small with a metal tip over an adsorbed CO on the surface or a CO tip over the bare metal surface according to IETS propensity rule [13,14]. Therefore, we attribute this peak to the overtone of the HR mode [22]. The HT and HR energies of CO on silver surfaces are lower than those on copper and gold surfaces [15], which can be correlated to the weaker binding [23] of CO on silver surfaces. All the vibrational modes for CO on the tip are redshifted from those of CO on the substrate, suggesting a weaker bonding of CO on the tip.

The asymmetry in the IETS line shapes is consistent with a previous study of asymmetric tunneling junctions [15]. The IETS spectrum taken with the CO tip over the center of the surface CO is shown at the bottom of Fig. 1(d). For this symmetric tunneling junction, the rising edge and falling tail of the HR mode (which is a mixture of the HR modes for tip CO and surface CO) in IETS show inversion symmetry for opposite sample bias polarities, in contrast to the spectrum for CO alone on the surface [top spectrum in Fig. 1(d)] or the tip [middle spectrum in Fig. 1(d)]. Intriguingly, in addition to the HT, HR, and overtone of the HR modes for single CO, an extra vibrational mode at 7.6 meV emerges in the CO dimer tunneling junction, as shown in the bottom spectrum in Fig. 1(d).

To study the evolution of this newly emerged vibrational mode, we took a series of vibrational d^2I/dV^2 spectra in Fig. 2(a) by tuning the tip-sample distance. The energies of the two vibrational modes (υ_α and υ_β) below 10 meV are plotted in Fig. 2(c) to highlight their variations over different tip-sample separations. The lower energy mode υ_α around 1.5 meV is found to be almost independent of the tip height. In contrast, the higher energy mode υ_β shows nonmonotonic variations. Mode υ_β blueshifts from 4.6 to 7.4 meV as ΔZ changes from −1.3 to 0.0 Å and saturates with further change in ΔZ from 0.0 to 0.8 Å. Most strikingly, the energy redshifts when the tip-sample distance is further reduced.

We calculated the vibrational modes of the double CO tunneling junction using a density functional approach with the van der Waals correction to gain understanding of the experimental observations [24]. Twelve vibrational modes were distinguished, as listed in Fig. S3. Remarkably, both CO molecules tilted away from the vertical orientation in the same XZ plane, and the hindered translation modes for the CO dimer are strongly coupled (υ_9 to υ_{12}). The out-of-phase coupling (optical) mode of the hindered translation of CO in the XZ plane has the highest energy (8.1 meV) among the four coupled translational vibrations. The other three translational modes have much lower energies (≤4.1 meV). All other vibrations have much higher energies (>10 meV). It is clear that the experimental υ_β mode stems from the out-of-phase mode (υ_9) that combines the hindered translations of two CO molecules in the XZ plane, and the υ_α mode should be a mixture of the other three coupled hindered translations. As a further support, the calculated energy of the υ_9 mode shows the same Z dependence in Fig. 3(a) as the experimental data [Fig. 2(c)].

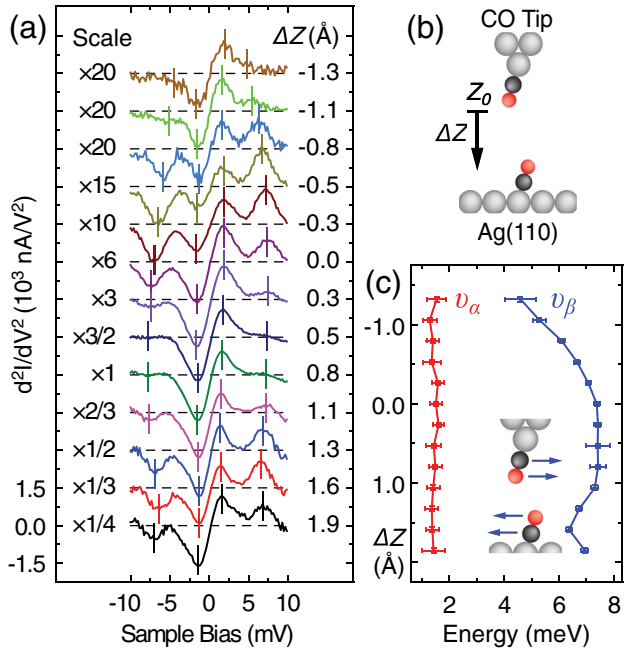

FIG. 2. Z-dependent STM-IETS. (a) A series of STM-IETS spectra at different tip-sample distances taken with the CO tip over the center of another CO adsorbed on Ag(110). The spectra are multiplied by different scale factors as indicated on the left side and offset vertically for better visualization. Sample bias modulation was 1.5 mV_{rms} at 311.11 Hz. (b) Schematic diagram of the CO tip over CO on Ag(110). Z_0 is the tunneling gap defined by $I = 80$ pA and $V = 10$ mV. For each spectrum, the tip feedback was turned off at Z_0, then the CO tip was advanced (positive values) or retracted (negative values) by ΔZ before making the measurement. (c) The vibrational energies extracted from (a) versus ΔZ. Error bars of energy reflect the uncertainty from Gaussian peak fitting; error bars of ΔZ (about 0.03 Å) reflect the tip height drift during the measurement and uncertainty of STM scanner ΔZ calibration. The higher energy mode υ_β is the out-of-phase coupled hindered translation as illustrated in the inset.

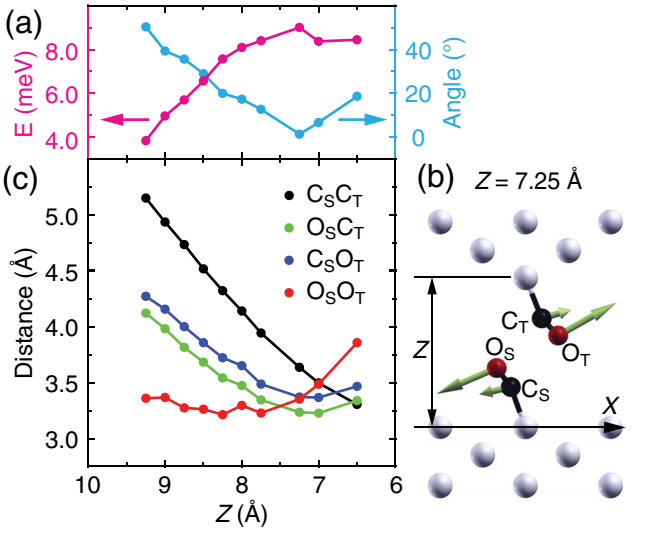

FIG. 3. (a) Calculated energy of coupled vibrational mode υ_9 (magenta curve) and the angle between $\overrightarrow{O_sO_t}$ and $(\overrightarrow{\nu_t^O} - \overrightarrow{\nu_s^O})$ (light blue curve) versus tip-sample distance Z. The energy reaches a maximum at $Z = 7.25$ Å. In the meantime, the $\overrightarrow{O_sO_t}$ is aligned with $(\overrightarrow{\nu_t^O} - \overrightarrow{\nu_s^O})$ and the angle between them approaches 0°. (b) Schematic diagram of the coupled mode eigenvector at $Z = 7.25$ Å; Z is defined as the vertical distance from the protruding Ag atom on the tip and the Ag surface layer before structure relaxation in the calculation. (c) Z dependence of distances between pairs of atoms in the two CO molecules.

Evidently, it is possible to use the new vibrational mode to probe the short range intermolecular interaction between the two CO molecules in the junction. Similar to LFM [8], the long range interaction between the macroscopic tip and surface does not contribute to the restoring force for the CO-CO lateral vibrations. From Fig. S4 it can be found that the two CO oscillation vectors are parallel and the oscillation amplitudes of oxygen atoms ($|\overrightarrow{\nu_t^O}|$ and $|\overrightarrow{\nu_s^O}|$) are much bigger than those of carbon atoms. Therefore, the coupling between CO molecules is governed by O-O repulsion, which can be estimated from O-O distance $|\overrightarrow{O_sO_t}|$ and the alignment of the relative vibration of the two oxygen atoms $(\overrightarrow{\nu_t^O} - \overrightarrow{\nu_s^O})$ with respect to $\overrightarrow{O_sO_t}$ [32]. When the tip CO approaches the other CO on the substrate, they push each other away from the vertical position. The $|\overrightarrow{O_sO_t}|$ does not drop linearly with Z as shown in Fig. 3(c); the angle between $\overrightarrow{O_sO_t}$ and $(\overrightarrow{\nu_t^O} - \overrightarrow{\nu_s^O})$ becomes smaller and the vibrational energy increases when Z is reduced as shown in Fig. 3(a). It is perceivable that the coupling between vibrations of two molecules is the strongest when $\overrightarrow{O_sO_t}$ aligns along $(\overrightarrow{\nu_t^O} - \overrightarrow{\nu_s^O})$ when Z reaches 7.25 Å and the vibrational energy is maximized. Further decrease of Z (to $Z < 7.25$ Å) causes expansion of $|\overrightarrow{O_sO_t}|$ and misalignment between $\overrightarrow{O_sO_t}$ and $(\overrightarrow{\nu_t^O} - \overrightarrow{\nu_s^O})$. As a consequence, the coupling between hindered translations of the two CO molecules weakens, and the energy of the optical mode decreases.

It is noticeable that the IETS intensity of υ_β also shows significant variation for different tip-sample distances as displayed in Fig. 2(a). At some tip heights ($\Delta Z = 0.3$, 0.5, and 0.8 Å) the IETS intensities of the υ_β mode are very weak. We plot the relative conductance change ($\Delta\sigma/\sigma$) due to the υ_β mode as a function of ΔZ in Fig. 4(a) to characterize the inelastic electron tunneling cross section. Based on this plot, we discern three regimes of CO-CO intermolecular coupling. Regime i and iii are separated by regime ii where the IETS cross section of υ_β is strongly suppressed.

The decrease of the IETS cross section in regime ii can be rationalized according to the IETS symmetry selection rules [33] or propensity rules [13,14]. The inelastic electron

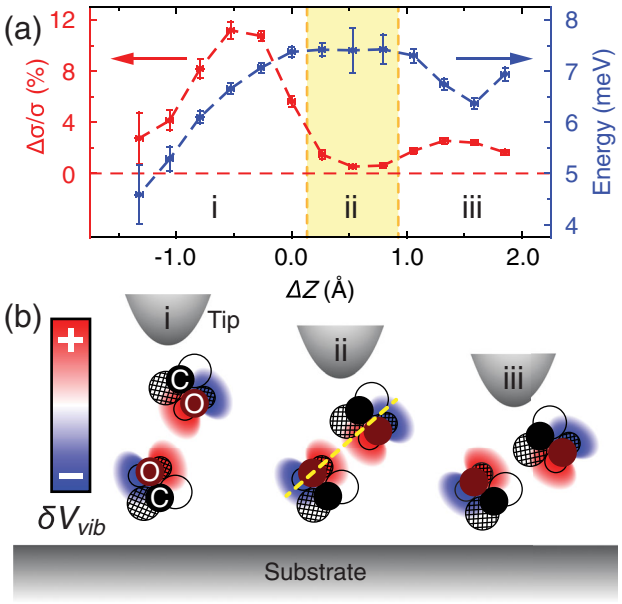

FIG. 4. (a) The relative conductance change $\Delta\sigma/\sigma$ as a function of ΔZ for mode υ_β. The vibrational energies are also shown to reveal the correlation between energy and IETS intensity. Three coupling regimes specified by i, ii, and iii are defined based on the IETS intensity of υ_β mode. Regime ii corresponds to lowest IETS intensity. (b) Schematic diagrams illustrating the interplay between the CO tilting angle and π orbital alignment of the two CO molecules in the junction. The opposite phases of the CO orbitals are indicted by open and gridded circles. The spatial distribution of the υ_β mode deformation potential δV_{vib} is depicted by color palette. Red and blue highlight the phase differences of δV_{vib}, which reflect the local symmetry of this out-of-phase coupled vibration.

tunneling rate derives from the spatial overlap of the tip and sample states (ψ_t and ψ_s) with the deformation potential (δV_{vib}) caused by the vibration. Because the deformation potential δV_{vib} is spatially localized in the tunneling junction, only the local symmetries of the tip and sample states of the few most transmitting eigenchannels determine their contributions to the overall inelastic tunneling process [13,14]. The inelastic tunneling cross section should be zero if $\psi_t \delta V_{\mathrm{vib}} \psi_s$ is antisymmetric about any symmetry planes. Previous studies indicate that the primary tunneling channels for CO tip over surface CO have the π character without considering the CO tilting [14,34]. Nevertheless, since only the $2\pi^*$ orbitals of CO are close to the Fermi level, even in a tilting tip-CO case [35], it is reasonable to assume that both the tip and sample states have the π character as shown in Fig. 4(b) in our experiment. The deformation potential of the υ_β is sketched in Fig. 4(b) to reveal its symmetry and spatial distribution. As mentioned earlier, oxygen atoms have much larger oscillation amplitude than carbon atoms, so the δV_{vib} is expected to be mostly localized on oxygen atoms.

With the reduction of tip-sample distance, the spatial overlap between tip and sample states is improved so that the IETS cross section is enhanced initially in regime i. As Z is further reduced, the cross section decreases and reaches its minimum in regime ii. This corresponds to the configuration that one lobe of the surface state is aligned with the nodal plane of the tip state as indicated by a yellow dashed line in Fig. 4(b), so that the product of ψ_t, ψ_s, and δV_{vib} is antisymmetric about that plane, which in turn gives rise to the attenuated IETS intensity. When the tip enters regime iii, the CO tilting angle continues to increase, causing the orbital lobe of the surface CO and orbital nodal plane of the tip-CO to become misaligned, allowing the υ_β IETS feature to appear again in Fig. 2(a).

In summary, we demonstrated the detection and identification of intermolecular coupled vibrations between a tip CO and surface CO through STM-IETS and first principles calculations. We rationalized the evolution of the vibration energy and IETS cross section as a function of tip-sample distance by considering the interplay between the CO bending and orbital alignment. The current study suggests a promising local probe to identify nonplanar chemical functional groups by detecting the coupled vibration between the CO tip and its interacting partners, providing a useful complement to the existing high resolution scanning probe techniques that focus on planar molecules. In addition, our findings indicate the possibility of quantitatively probing intermolecular interaction and the origin of more complex group excitations such as phonons from coupled vibrational modes in molecular junctions.

This work was supported by the Condensed Matter Physics Program, Division of Materials Research, National Science Foundation, under Grant No. DMR-1411338.

*To whom all correspondence should be addressed.
wilsonho@uci.edu

[1] J. T. Yates, Surf. Sci. **299**, 731 (1994).
[2] L. Gross, F. Mohn, N. Moll, P. Liljeroth, and G. Meyer, Science **325**, 1110 (2009).
[3] D. G. de Oteyza, P. Gorman, Y.-C. Chen, S. Wickenburg, A. Riss, D. J. Mowbray, G. Etkin, Z. Pedramrazi, H.-Z. Tsai, A. Rubio, M. F. Crommie, and F. R. Fischer, Science **340**, 1434 (2013).
[4] J. Zhang, P. Chen, B. Yuan, W. Ji, Z. Cheng, and X. Qiu, Science **342**, 611 (2013).
[5] C.-L. Chiang, C. Xu, Z. Han, and W. Ho, Science **344**, 885 (2014).
[6] Z. Sun, M. P. Boneschanscher, I. Swart, D. Vanmaekelbergh, and P. Liljeroth, Phys. Rev. Lett. **106**, 046104 (2011).
[7] A. Schwarz, A. Köhler, J. Grenz, and R. Wiesendanger, Appl. Phys. Lett. **105**, 011606 (2014).
[8] A. J. Weymouth, T. Hofmann, and F. J. Giessibl, Science **343**, 1120 (2014).
[9] B. C. Stipe, M. A. Rezaei, and W. Ho, Science **280**, 1732 (1998).

[10] S. Li, D. Yuan, A. Yu, G. Czap, R. Wu, and W. Ho, Phys. Rev. Lett. **114**, 206101 (2015).
[11] J. Guo, J.-T. Lu, Y. Feng, J. Chen, J. Peng, Z. Lin, X. Meng, Z. Wang, X.-Z. Li, E.-G. Wang, and Y. Jiang, Science **352**, 321 (2016).
[12] D. Yuan, Z. Han, G. Czap, C.-L. Chiang, C. Xu, W. Ho, and R. Wu, J. Phys. Chem. Lett. **7**, 2228 (2016).
[13] M. Paulsson, T. Frederiksen, H. Ueba, N. Lorente, and M. Brandbyge, Phys. Rev. Lett. **100**, 226604 (2008).
[14] A. Garcia-Lekue, D. Sanchez-Portal, A. Arnau, and T. Frederiksen, Phys. Rev. B **83**, 155417 (2011).
[15] C. Xu, C.-L. Chiang, Z. Han, and W. Ho, Phys. Rev. Lett. **116**, 166101 (2016).
[16] M. Persson, Phil. Trans. R. Soc. A **362**, 1173 (2004).
[17] J. R. Hahn and W. Ho, Phys. Rev. Lett. **87**, 196102 (2001).
[18] B. C. Stipe, M. A. Rezaei, and W. Ho, Rev. Sci. Instrum. **70**, 137 (1999).
[19] L. Bartels, G. Meyer, and K.-H. Rieder, Appl. Phys. Lett. **71**, 213 (1997).
[20] N. Lorente and H. Ueba, Eur. Phys. J. D **35**, 341 (2005).
[21] J. Oh, H. Lim, R. Arafune, J. Jung, M. Kawai, and Y. Kim, Phys. Rev. Lett. **116**, 056101 (2016).
[22] This mode has been identified as the overtone of the CO HR mode by high energy resolution STM-IETS meaurement at 600 mK.
[23] A. Föhlisch and H. P. Bonzel, in *Adsorbed Layers on Surfaces*, edited by H. P. Bonzel (Springer-Verlag, Berlin, 2005), p. 88.
[24] See Supplemental Material at http://link.aps.org/supplemental/10.1103/PhysRevLett.118.036801 for more details, which includes Refs. [25–31].
[25] G. Kresse and J. Furthmüller, Phys. Rev. B **54**, 11169 (1996).
[26] G. Kresse and J. Furthmüller, Comput. Mater. Sci. **6**, 15 (1996).
[27] G. Kresse and D. Joubert, Phys. Rev. B **59**, 1758 (1999).
[28] H. J. Monkhorst and J. D. Pack, Phys. Rev. B **13**, 5188 (1976).
[29] S. Grimme, J. Antony, S. Ehrlich, and H. Krieg, J. Chem. Phys. **132**, 154104 (2010).
[30] S. Grimme, S. Ehrlich, and L. Goerigk, J. Comput. Chem. **32**, 1456 (2011).
[31] J. Klimeš, D. R. Bowler, and A. Michaelides, J. Phys. Condens. Matter **22**, 022201 (2010).
[32] The repulisve force along the eigenvector for the coupled vibration is proportional to $[V(|\vec{r}+dt\times\overrightarrow{\nu_t^O}-dt\times\overrightarrow{\nu_s^O}|)-V(r)]/dt=\partial V(r)/\partial r(\overrightarrow{\nu_t^O}-\overrightarrow{\nu_s^O})\cdot(\vec{r}/r)$, where $\vec{r}=\overrightarrow{O_tO_s}$, $r=|\vec{r}|$, and $V(r)$ is the interatomic potential between the two oxygen atoms. Therefore, the O-O repulsion is a function of $|\overrightarrow{O_sO_t}|$ and the angle between $(\overrightarrow{\nu_t^O}-\overrightarrow{\nu_s^O})$ and $\overrightarrow{O_sO_t}$.
[33] N. Lorente, M. Persson, L. J. Lauhon, and W. Ho, Phys. Rev. Lett. **86**, 2593 (2001).
[34] A. Gustafsson and M. Paulsson, Phys. Rev. B **93**, 115434 (2016).
[35] M. Corso, M. Ondráček, C. Lotze, P. Hapala, K. J. Franke, P. Jelínek, and J. I. Pascual, Phys. Rev. Lett. **115**, 136101 (2015).